Rotationally Inelastic Scattering of Quantum-State Selected ND_3 with Ar

Ondřej Tkáč,[a] Ashim K. Saha,[b] Jérôme Loreau,[c] David H. Parker,*[b] Ad van der Avoird,*[b] and Andrew J. Orr-Ewing*[d]

[a] *Laboratorium für Physikalische Chemie, ETH Zürich, CH-8093 Zürich, Switzerland*

[b] *Radboud University Nijmegen, Institute for Molecules and Materials, Toernooiveld 1, 6525ED Nijmegen, The Netherlands*; E-mail: parker@science.ru.nl, avda@theochem.ru.nl

[c] *Service de Chimie Quantique et Photophysique, Université Libre de Bruxelles (ULB) CP 160/09, 50 av. F.D. Roosevelt, 1050 Brussels, Belgium*

[d] *School of Chemistry, University of Bristol, Cantock's Close, Bristol BS8 1TS, UK*; E-mail: a.orr-ewing@bris.ac.uk

Abstract

Rotationally inelastic scattering of ND_3 with Ar is studied at mean collision energies of 410 and 310 cm^{-1}. In the experimental component of the study, ND_3 molecules are prepared by supersonic expansion and subsequent hexapole state selection in the ground electronic and vibrational levels and in the $j_k^{\pm} = 1_1^-$ rotational level. A beam of state-selected ND_3 molecules is crossed with a beam of Ar, and scattered ND_3 molecules are detected in single final $j'^{\pm}_{k'}$ quantum states using resonance enhanced multiphoton ionization spectroscopy. State-to-state differential cross sections for rotational-level changing collisions are obtained by velocity map imaging. The experimental measurements are compared with close-coupling quantum-mechanical scattering calculations performed using an *ab initio* potential energy surface. The computed DCSs agree well with the experimental measurements, confirming the high quality of the potential energy surface. The angular distributions are dominated by forward scattering for all measured final rotational and vibrational inversion symmetry states. This outcome is in contrast to our recent results for inelastic scattering of ND_3 with He, where we observed significant amount of sideways and backward scattering for some final rotational levels of ND_3. The differences between He and Ar collision partners are explained by differences in the potential energy surfaces that govern the scattering dynamics.

I. Introduction

Prior study of rotational energy transfer in collisions of ammonia isotopologues with He and H_2 has been motivated by astrophysical applications,[1-4] as discussed in our recent paper.[5] To complement such studies, and to examine the effects of changes to the properties of the collision partner on the collision dynamics, inelastic scattering of NH_3 with Ar has also been the subject of extensive previous experimental investigation.[6-9] This paper presents the first quantum state-to-state resolved differential cross sections (DCSs), as well as calculated integral cross sections (ICS) for the ND_3 + Ar system. The objectives are to explore the dynamics of translational to rotational energy transfer for this system, and thereby to derive insights into the intermolecular interactions between these colliding species. The state-resolved ICSs and DCSs are sensitive to the anisotropy of the intermolecular interactions and can be used to test computed potential energy surfaces (PESs) and quantum mechanical (QM) scattering calculations that simulate the collision dynamics. ICSs do not allow ready distinction of the influence of the short range repulsive and the long range attractive parts of the PES,[3, 8] so important additional insights are gained from measurement of the angular distribution of particles scattered into a specific final state.

A DCS determination offers more detailed information about the PES governing the collisions than is contained in the ICS, since the form of the DCS can reveal the dependence of the collision dynamics on the impact parameter, b. The $\chi \sim V(b)/E_{\mathrm{coll}}$ relationship, where $V(b)$ is interaction potential and E_{coll} is the collision energy, illustrates that forward scattering (corresponding to small deflection angles χ) originates from large impact parameters and hence samples the attractive long-range part of the potential. Rainbow scattering occurs when a trajectory samples the minimum of the potential, which may correspond to a well resulting from van der Waals interactions, and the large deflections characteristic of backward scattering originate from collisions at small impact parameters that probe the short range part of the PES.

In addition to extending the understanding of the intermolecular interaction between ND_3 and Ar, the results presented in this paper are contrasted with the collisional scattering behaviour of ND_3 with Ne,[10] and He.[5] In this way, the effect of mass, polarizability and duration of the interaction can be explored for collisions of ND_3 with He, Ne and Ar. With selection of ND_3 in a single vibrational and rotational level and the antisymmetric component of the umbrella vibrational inversion doublet prior to collisions, we are able to make precise measurements of the scattering that are not degraded by averaging over an initial distribution of states.

Prior determinations of DCSs for rotationally inelastic scattering were reported, for example, for H_2O collisions with He[11-12] and H_2,[13] OH radical with Ar and He,[14] HCl with various colliders,[15] and NO with Ar and He.[16-20] Recently, the inelastic scattering dynamics of methyl radical with He,[21] H_2 and D_2,[22] and Ar[23] were examined using crossed molecular beam

methods in combination with velocity map imaging (VMI). Measured DCSs were contrasted with theoretical DCSs calculated using quantum mechanical close-coupling scattering calculations on newly computed *ab initio* PESs. Excellent agreement lends confidence to the quality of the calculated PESs. These studies also explored the effects of anisotropies in the intermolecular potential associated with the polar and azimuthal angles of approach of the collision partner, defined with respect to the three-fold rotational symmetry axis of the methyl radical. Comparisons have been made between the scattering dynamics of the planar, open-shell CD_3 radical and the pyramidal, closed-shell ND_3 molecule in collisions with He on the basis of rigorous close-coupling scattering calculations.[24] There are many similarities between the DCSs for ND_3–He (for collisions that conserve the ± symmetry) and CD_3–He scattering, nevertheless observed differences can be linked to interaction terms in the expansion of the PES which directly couple transitions between initial and final rotational levels.

The ND_3 molecule is an important candidate for potential applications in experimental studies of cold collisions. In crossed beam scattering experiments, a Stark decelerator can be used to decelerate neutral polar molecules with a time-varying electric field. The inelastic scattering can be studied over a wide range of collision energies. In this way, the details of scattering processes that remain hidden in conventional crossed beam scattering experiments may be revealed. For example, the effects of Feshbach and shape resonance can be observed, as can the diffraction oscillation present in the small angle scattering of the DCSs, which are beyond the resolution of the current experiments. Diffraction oscillations were recently resolved in inelastic scattering experiments of a Stark decelerated beam of NO with He, Ne and Ar.[25] The signatures of scattering resonances have been studied theoretically for the NH_3 – He system.[26]

In this paper, results are presented for the state-to-state scattering of ND_3, prepared in its ground electronic and vibrational levels and in the $j_k^{\pm} = 1_1^-$ rotational level, with Ar at two collision energies 410 ± 40 $cm^{-1}$and 310 ± 30 cm^{-1}. Initial state selection is achieved by supersonic expansion and hexapole state selection. In addition to the experiments performed with the hexapole state selected $ND_3(1_1^-)$ scattered by Ar, velocity map images were measured for ND_3 – Ar without use of the hexapole, for scattering into final levels with j' = 2 and 3, with the initial state averaged over several rotational levels populated in the molecular beam expansion. Experimental DCSs are compared to theoretical DCSs calculated using the close-coupling method on an accurate *ab initio* PES.

II. Method

A. Experimental apparatus

All experimental measurements were conducted in a crossed molecular beam instrument equipped with velocity map imaging capability located in the Nijmegen laboratory. The experimental apparatus has been described previously, and we provide only a summary here.[5] A primary beam of 1% ND_3 diluted in Ar or Kr and a secondary beam of pure Ar were crossed at 90^o in a vacuum chamber. The scattered ND_3 molecules were probed using (2+1) REMPI spectroscopy via the $\widetilde{B}$-state. The ions were projected onto a position sensitive detector using VMI ion optics, generating a 2D projection of the 3D distribution of velocities resulting from the inelastic scattering. A UV laser was tuned to specific vibrational and rotational features in the (2+1) REMPI spectrum of ND_3 in order to generate velocity map images for ND_3 molecules populating individual rotational and inversion symmetry levels of the lowest vibrational state. Prior to collisions with Ar, the ND_3 was cooled in a supersonic expansion to its ground vibrational and low-lying rotational levels, and was passed through a hexapole filter, giving full initial j, k and umbrella inversion symmetry selection. Further details of the selection of initial quantum states, ND_3 rotational levels and spectroscopy of the $\widetilde{B} \leftarrow \widetilde{X}$ transition used to detect the scattered ND_3 can be found elsewhere.[5]

Conversion of raw images to centre-of-mass (CM) frame differential cross sections requires a density-to-flux transformation that corrects for the experimental bias towards observation of slower moving ND_3 products in the laboratory frame. The density-to-flux conversion was carried out using two separate and independent computer programs. The IMSIM program of McBane[27] employs an iterative correction to the raw experimental images, whereas our adapted version of the program of Eyles and Brouard[28] uses a Monte Carlo method to simulate the effects of the experimental design on the preferential detection of certain subsets of the scattered ND_3. Further discussion of the density-to-flux procedure is given in the Supplementary Information. The DCSs extracted by the Monte Carlo and IMSIM method are in very good agreement as can be seen in Fig. S1. Such good agreement in all cases imparts confidence in the process for extraction of DCSs from the experimental images. Since the IMSIM and Monte Carlo programs give the same DCSs, in the following sections we present only DCSs extracted by the Monte Carlo simulation program.

B. Potential energy surface

The scattering calculations were carried out on the recent potential energy surface of Loreau *et al.*[29] This PES depends on four coordinates R, θ, ϕ, and ρ. The position of the Ar atom relative to the center of mass of ND_3 is defined by the vector **R** of length R, while θ (with $0 \leq \theta \leq \pi$) is the angle between the vector **R** and the C_3 axis of ND_3, and ϕ (with $0 \leq \phi \leq 2\pi$) is the angle of rotation of this vector around the C_3 axis. ρ is the angle between the C_3 axis of ND_3 and the ND bonds and describes the umbrella inversion motion of ND_3. The ND bonds were

kept frozen at 1.9204 a_0. While the interaction energies were computed in a coordinate system with the origin on the N atom, the transformation to the center of mass coordinate system can be achieved using Eqs. (1) and (2) of Ref. [29].

The PES was calculated at 6820 geometries by means of the coupled-cluster method with single, double, and perturbative triple excitations (CCSD(T)) with the aug-cc-pVQZ basis set augmented by a set of (3*s*3*p*2*d*2*f*1*g*) mid-bond functions. Scalar relativistic effects were included through the Douglas-Kroll-Hess Hamiltonian and the energy was corrected for the basis set superposition error at each geometry. Further details are available in Ref. [29].

The PES was expanded in tesseral spherical harmonics $S_{\lambda\mu}(\theta,\phi)$:

$$V(R,\theta,\phi,\rho) = \sum_{\lambda,\mu} v_{\lambda\mu}(R,\rho) S_{\lambda\mu}(\theta,\phi) \quad (1)$$

The functions $S_{\lambda\mu}(\theta,\phi)$ are real-valued combinations of spherical harmonics $Y_{\lambda\mu}(\theta,\phi)$ defined by $S_{\lambda\mu}(\theta,\phi) = \{(-1)^{\mu} Y_{\lambda\mu}(\theta,\phi) + Y_{\lambda,-\mu}(\theta,\phi)\}/\sqrt{2}$ for $\mu>0$, with $S_{\lambda 0}(\theta,\phi) = Y_{\lambda 0}(\theta,\phi)$, and the expansion coefficients depend on R and ρ The R-dependence of the functions $v_{\lambda\mu}(R,\rho)$ was fitted using cubic splines in the interaction region ($R \leq 30$ a_0) and the appropriate inverse powers of R in the long-range region ($R > 30$ a_0) (see Ref. [29]). Their dependence on the umbrella angle ρ was fitted to a polynomial expansion.

The PES has been used in Ref. [29] to compute the bound states of the van der Waals complexes NH_3–Ar and ND_3–Ar. For both complexes, excellent agreement was observed between the theoretical calculations and the experimental data for the energies and rotational constants of the bound rovibrational states, demonstrating the quality of the PES.

C. Quantum scattering calculations

The scattering calculations were performed by means of the close-coupling (CC) method[30] in the body-fixed frame. The second-order close-coupled equations are diagonal in the total angular momentum J and its projection M_J on the space-fixed z-axis.

Since the PES of ND_3–Ar depends on the angle ρ, the umbrella inversion motion of ND_3 could be treated explicitly in our calculations. The wave functions and energy levels corresponding to ND_3 inversion were computed using a ρ-dependent Hamiltonian. It contains the kinetic energy operator corresponding to the inversion motion as well as a double-well potential[5, 26] $V(\rho)$ fitted in order to reproduce accurately the experimental tunneling frequencies (0.053 cm^{-1} and 3.50 cm^{-1}, respectively) in the ground ($v = 0$) and first excited ($v = 1$) umbrella vibrational states, as well as the $v = 0 \rightarrow 1$ excitation frequency of 747.3 cm^{-1}. We included the lowest four inversion levels (corresponding to $v = 0$ and $v = 1$) in the scattering calculations.

The CC equations were solved for two collision energies (310 cm^{-1} and 410 cm^{-1}) using the renormalized Numerov algorithm on an equidistant grid of 250 points ranging from R = 4.3 a_0 to R = 22 a_0. All rotational states of ND_3 up to j = 11 were included in the basis set and all partial waves up to a total angular momentum of J = 120 were taken into account. The cross sections were converged to within 1% with respect to all parameters. The masses are 2.014101778 u for D, 14.003074 u for ^{14}N and 39.962383 u for ^{40}Ar.

III. Results and Discussion

A. Integral cross sections

Fig. 1 shows calculated integral cross sections for ND_3 collisions with Ar from the initial level $j_k^{\pm} = 1_1^-$ to final rotational levels $j'^{\pm}_{k'}$ up to $j' = 6$. For a final level with a given $j'_{k'}$, the $\pm$ umbrella inversion symmetry has a significant effect on the magnitude of the ICS. For ND_3 final levels with – inversion symmetry, 80 % of the scattering produces $j' \leq 4$, whereas this fraction is 51 % for + inversion symmetry final levels. The observed propensities arise because inversion symmetry conserving transitions are directly coupled by expansion coefficients $v_{\lambda\mu}$ for which $\lambda + \mu$ is even ($\lambda, \mu \geq 0$), whereas for inversion symmetry changing transitions $\lambda + \mu$ must be odd.[31] The size of the expansion coefficient then determines the magnitude of the ICS. The coefficients $v_{\lambda\mu}$ are plotted as a function of the internuclear distance R in Fig. 5 of Ref. [29]. The most significant contributions to the expansion in Eq. (1) over the R-range of importance to the inelastic scattering are from the v_{00} coefficient, which describes the isotropic part of the PES, the v_{10} (and to a lesser extent v_{20} and v_{30}) terms that describe the θ-dependence, and v_{33} and v_{43} which are the first terms that describe the ϕ dependence.

Certain trends in the ICS values are highlighted here. The 2_2^+ and 5_5^+ final levels are not directly coupled to the initial 1_1^- level by any expansion coefficients (but are instead linked by a combination of terms) and therefore the associated ICSs are very small. For 2_1, 3_1 and 4_1 final levels, the ICSs are larger for the – symmetry component of the final state. These transitions are directly coupled by $v_{\lambda 0}$ coefficients. On the other hand, the transitions into 3_2, 4_2 and 5_2 final levels have larger ICSs for the + symmetry final state. These symmetry changing transitions are directly coupled by the v_{43} coefficient (and the v_{63} coefficient in the case of the 5_2 level), as opposed to symmetry conserving transitions (– symmetry of the final level) which are directly coupled by the v_{33} or v_{53} coefficient. The ICS for the 4_4 final level is larger for – symmetry, because it is directly coupled by two expansion coefficients v_{33} and v_{53},

whereas the 4_4^+ final level is directly coupled only by the v_{43} coefficient. Similarly the 5_4^+ final level with a large calculated ICS is directly coupled by v_{63} and v_{43} terms, whereas the 5_4^- final state is only linked to the initial 1_1^- level by the v_{53} coefficient. Similar arguments can be made for higher $j'^{\pm}_{k'}$ final levels.

B. Differential cross sections for ND_3 (1_1^-) + Ar scattering

Measurements of the dynamics of the ND_3 – Ar system were made at two different collision energies by seeding the ND_3 molecules either in Ar or Kr. The collision energy for inelastic scattering of ND_3 seeded in Ar with a second Ar beam was 410 ± 40 cm^{-1}, while with krypton as a carrier gas the collision energy was 310 ± 30 cm^{-1}. Fig. 2 shows velocity map images for experiments using the hexapole state selection to prepare ND_3 (1_1^-) molecules seeded in Ar. The images for Kr as a carrier gas can be found in the Supplementary information. The DCSs were extracted from raw images using the Monte Carlo density-to-flux conversion code. The resultant DCSs for state-to-state scattering of ND_3 ($j_k^{\pm} = 1_1^-$) at 410 and 310 cm^{-1} are displayed in Figs. 3 and 4 for numerous final $j'^{\pm}_{k'}$ quantum states. The experimental DCSs are compared with theoretical DCSs; for the purposes of the comparison, the experimental data were normalized to match the computed DCS values at a scattering angle of 45°.

All the measured DCSs for collisions of ND_3 with Ar are dominated by forward scattering, suggesting an important role of the long-range attractive part of the PES in determining the outcomes of collisions. With closer examination, we notice fine differences between DCSs (in particular, the calculated versions) between individual final levels. Most of the DCSs show a sharp decrease toward larger scattering angles and do not extend significantly behind $\theta \sim 50^o$. In these cases, excellent agreement between experimental and calculated DCSs is found, except that the computed diffraction oscillations are not resolved in our experiments. Several calculated DCSs for final levels $j'^{\pm}_{k'} = 5_5^-$ and 7_7^- (coupled to $j_k^{\pm} = 1_1^-$ by the v_{66} coefficient) as well as for $3_2^+, 4_2^+$ and 4_4^+ (coupled by the v_{43} coefficient) show very sharp forward peaks extending only up to $\theta \sim 10^o$ and then a broad shoulder up to $\theta \sim 120^o$. For these final levels, the agreement with experiment is somewhat poorer. In particular, the experimental DCSs do not show the two resolved features, but instead have a forward peak extending up to $\theta \sim 90^o$ that is broader than for the remainder of the final levels. The disagreement could be explained by insufficient angular resolution in our experiment, which smears out the sharp forward peak and merges the two features observed in the calculated DCSs into one broad peak.

Alternatively, it could signal a modest inadequacy of the description of the interaction potential between ND_3 and Ar by the current PES, resulting in inaccurate determination of the v_{43} and v_{66} coefficients. We suggest that the former explanation is the more likely. The most pronounced sideways scattering shoulder is predicted by calculation for the DCS for $j'^{\pm}_{k'} = 3^+_2$, and this is reproduced well by the experiment. Also notice that DCSs for final levels 3^+_1 and 4^+_1 (coupled to $j^{\pm}_k = 1^-_1$ by the v_{30} coefficient) show, in addition to a sharp forward peak, a minimum around $\theta \sim 45^o$ followed by a slight increase toward large scattering angles (sideways and backward scattering). This fine feature is also well reproduced in the experiment probing the 4^+_1 final level, but is not seen for the 3^+_1 image. The $j'^{\pm}_{k'} = 2^+_2$ final level is not directly coupled to $j^{\pm}_k = 1^-_1$ by any expansion coefficient of the PES, which is why the vertical scale for the DCS is much smaller than for other final states, and the diffraction oscillations in the calculated DCS are not so pronounced. A shift toward larger scattering angles (*i.e.*, backward scattering) for ND_3 + Ar is predicted by theory for final rotational levels starting with $j' = 6$.

Of the measured final levels, the 3_2, 4_2 and 4_4 final levels are also of interest because they exhibit the largest difference between DCSs for ND_3 products having the same rotational quantum numbers, but differing in + and − symmetry components. In contrast to the shapes of DCSs for + symmetry components with a sharp forward peak and broad shoulder, the DCSs for − symmetry components are much narrower and confined more in the forward hemisphere. In addition, the DCSs for final rotational levels 4^+_1 and 5^-_4 are much more strongly forward peaking than those for 4^+_2 and 5^-_5 levels, which differ only in the k' projection quantum numbers and thus by different expansion coefficients that directly couple these final levels.

The change in the collision energy for inelastic scattering of ND_3 with Ar from 410 ± 40 cm^{-1} (Ar carrier gas) to 310 ± 30 cm^{-1} (Kr carrier gas) has no apparent effect on the shapes of the DCS and hence the collision dynamics. The signal level for the 7^-_7 final level was too low to measure an experimental image for the lower collision energy of 310 ± 30 cm^{-1}.

C. Differential cross sections for +/− symmetry averaged ND_3 + Ar scattering

In addition to the experiments performed with the hexapole state selected ND_3 (1^-_1) scattered by Ar, velocity map images were measured for ND_3 – Ar without use of the hexapole. Fig. S4 shows images for scattering into final levels with j' = 2 and 3. State selective detection was carried out solely through the $\tilde{B}(5)$ band, therefore the umbrella inversion symmetry of the final level for all measured images is –. The ND_3 was rotationally cooled in a supersonic expansion but was not subjected to further rotational level or umbrella inversion symmetry

selection in a hexapole filter. The initial population of the beam is averaged over several rotational levels and inversion symmetries of ND_3. Only levels with the same nuclear spin symmetry can be considered as initial levels for production of a particular final level of that spin symmetry. The initial level populations of ND_3 at 4 K are listed in Table 1 in Ref. [5]. For the *E* nuclear spin modification (final levels 2_1^-, 3_1^- and 3_2^-), the initial state is $j_k = 1_1$, but +/– symmetry averaged, whereas the initial states for A_1 symmetry are $j_k^{\pm} = 0_0^+$ and 1_0^- and for the A_2 modifications are $j_k^{\pm} = 0_0^-$ and 1_0^+. The final level 2_0^- corresponds to the A_2 modification and 3_0^- to the A_1 modification of ND_3. The collision energy was 415 ± 40 cm^{-1}, which is slightly larger than for hexapole state selected experiments described in the previous sections because a different pulsed valve (Jordan instead of Nijmegen pulsed valve) was used to produce the primary ND_3 beam. This change of valve resulted in a slightly larger velocity of the ND_3 beam.

The DCSs extracted from experimental velocity map images are shown in Fig. 5 for j' = 2 and 3, and are compared to calculated DCSs averaged over appropriate initial level distributions. The experimental DCSs are normalized to match the values of the computed DCSs at 45°. All measured DCSs peak in the forward hemisphere with a maximum at θ = 0º, similar to the observed DCSs for scattering of hexapole state selected $ND_3(1_1^-)$ with Ar. However, the DCSs measured for +/– symmetry averaged initial levels of ND_3 extend as far as θ = 90º, in contrast to DCSs for the 1_1^- initial level of ND_3, which extend only up to θ = 45º. Although the unfiltered molecular beam contains ND_3 populating levels other than 1_1^-, computed DCSs suggest the broadened angular scattering observed experimentally cannot simply be accounted for by contributions from scattering out of these other levels.

D. Comparison of ND_3 scattering with rare gases

The scattering dynamics of $ND_3(1_1^-)$ – Ar can be compared to previously reported ICSs and DCSs for $ND_3(1_1^-)$ scattering by He.[5] Fig. 6 compares ICSs for these systems for scattering out of $j_k^{\pm} = 1_1^-$ to various final rotational levels $j'_{k'}$ at a collision energy 410 cm^{-1} for both systems. In general the ICSs are larger for Ar as a collision partner than for He, especially for final ND_3 levels with + umbrella inversion symmetry (Fig. 6(b)). For inelastic scattering of ND_3 out of the $j_k^{\pm} = 1_1^-$ level with He, 78 % of collisions conserve the umbrella inversion symmetry, whereas this fraction is only 58 % for Ar. The total inelastic ICS out of the ND_3

$j_k^{\pm} = 1_1^-$ level for collisions with He is only 40 % of the corresponding ICS for Ar collisions at this energy.

Example DCSs for inelastic scattering of ND_3 with Ar and He into a few selected $j'^{\pm}_{k'}$ final levels are overlaid in Fig. 7. These DCSs were calculated at a collision energy 410 cm^{-1} for both systems. The DCSs clearly demonstrate that scattering with Ar is in general more sharply peaking in the forward hemisphere than for He, for which the distributions are broader with more sideways or backward scattering, even for the low lying final levels. The same conclusion has recently been drawn for inelastic scattering of CD_3 with Ar and He,[23] for which the differences were traced to features of the PESs that govern the scattering dynamics. Corresponding differences in the PESs can also explain the scattering dynamics of ND_3 with Ar and He. Cuts through the minimum geometry of the ND_3 – Ar and ND_3 – He PESs are shown in Fig. 8. The global minimum of the PES is located at R = 6.756 bohr with a well depth of D_e = 147.6 cm^{-1} for ND_3 – Ar, whereas for ND_3 – He the minimum occurs at a smaller distance R = 6.095 bohr with a substantially shallower well, D_e = 35 cm^{-1}. Longer-range attractive interactions are more significant in the ND_3 – Ar system than for ND_3 – He, and larger impact parameter collisions lead to the observed forward scattering.

The DCSs for $ND_3(1_1^-)$ scattering by He into final levels $j'^-_{k'}$ and $j'^+_{k'}$, differing only in the umbrella inversion symmetry of the final level, exhibit distinctly different behaviour. In contrast, the DCSs for $ND_3(1_1^-)$ – Ar have, in general, very similar shapes for scattering into both final levels $j'^-_{k'}$ and $j'^+_{k'}$. In other words, the DCSs for $ND_3(1_1^-)$ – Ar for a given transition, differing only in whether the +/– symmetry is conserved or changes during a collision, are nearly identical in shape, but not in magnitude.

Experimental DCSs for inelastic scattering of ND_3 from neon as a collision partner have only been presented previously for ND_3 prepared in +/– symmetry averaged initial levels.[10] The DCSs for the ND_3 - Ne system are forward peaking for $j' \leq 4$ and sideways and backward scattered for higher j', as is the case of He. The scattering from Ne therefore contrasts with Ar scattering, which is dominated by forward scattering for all measured final levels.

IV. Conclusions

The angular distributions of 1_1^- state-prepared ND_3 scattered by Ar are dominated by forward scattering for all measured final rotational and umbrella inversion symmetry states. This outcome contrasts with our prior studies of ND_3 scattered by He, for which the DCSs are

broader and, for higher j', are dominated by sideways and backward scattering. These differences are attributed to the attractive versus repulsive character of the PESs governing the scattering dynamics.

Fully state-to-state DCSs for inelastic scattering of ND_3 ($\tilde{X}$, $\nu = 0, j_k^{\pm} = 1_1^-$) with Ar at collision energies of 310 and 410 cm^{-1} were compared to DCSs obtained by quantum mechanical scattering calculations performed using an *ab initio* PES. The comparisons show good agreement for selected final rotational levels up to $j'_{k'} = 7_7$ and for both symmetric (+) and antisymmetric (–) components of the inversion vibration associated with the ν_2 umbrella mode of ND_3. The DCSs for ND_3 scattered by Ar from the 1_1^- level into $j'^{+}_{k'}$ and $j'^{-}_{k'}$ inversion vibrational states are nearly identical in shape, with the exception of the measured 3_2, 4_2 and 4_4 final levels, while the magnitude (ICSs) is different even for other final levels.

Acknowledgements

The Nijmegen group acknowledges financial support from NWO-CW ECHO (for A.S.). The Bristol group thanks EPSRC for funding via the EPSRC Programme Grant EP/G00224X. Both groups were part of the EU Initial Training Network *ICONIC* which provided financial support for O.T. and for visits between the two institutions. J. Loreau acknowledges support from the Fonds de la Recherche Scientifique – FNRS, and the Wiener-Anspach foundation.

Supporting Information Available

Supporting Information provides a description of the density-to-flux transformation of data from velocity map images to obtain differential cross sections, velocity map images for ND_3 (1_1^-) + Ar scattering at a collision energy of 310 ± 30 cm^{-1}, and images for ND_3 + Ar scattering without the use of the hexapole filter for ND_3 state selection at a collision energy of 415 ± 40 cm^{-1}. This information is available free of charge via the Internet at http://pubs.acs.org

References

(1) Ebel, G.; Krohne, R.; Buck, U.; Schinke, R., Differential Molecular-beam Scattering Cross-sections as a Probe of the NH_3-H_2 Potential Surface. *J. Phys. Chem.* **1991,** *95*, 8232-8235.

(2) Ebel, G.; Krohne, R.; Meyer, H.; Buck, U.; Schinke, R.; Seelemann, T.; Andresen, P.; Schleipen, J.; ter Meulen, J. J.; Diercksen, G. H. F., Rotationally Inelastic-scattering of

NH_3 with H_2 - Molecular-beam Experiments and Quantum Calculations. *J. Chem. Phys.* **1990,** *93*, 6419-6432.

(3) Meyer, H., State-resolved Cross-sections and Collision-induced Alignment from Counterpropagating Beam Scattering of NH_3+He. *J. Phys. Chem. A* **1995,** *99*, 1101-1114.

(4) Seelemann, T.; Andresen, P.; Schleipen, J.; Beyer, B.; ter Meulen, J. J., State-to-state Collisional Excitation of NH_3 By He and H_2 Studied in a Laser Crossed Molecular-beam Experiment. *Chem. Phys.* **1988,** *126*, 27-45.

(5) Tkáč, O.; Saha, A. K.; Onvlee, J.; Yang, C.-H.; Sarma, G.; Bishwakarma, C. K.; van de Meerakker, S. Y. T.; van der Avoird, A.; Parker, D. H.; Orr-Ewing, A. J., State-to-state Resolved Differential Cross Sections for Rotationally Inelastic Scattering of ND3 with He. *Phys. Chem. Chem. Phys.* **2014,** *16*, 477-488.

(6) Meyer, H., Counterpropagating Pulsed Molecular-beam Scattering of NH_3-Ar . 1. State-resolved Integral Cross-sections. *J. Chem. Phys.* **1994,** *101*, 6686-6696.

(7) Meyer, H., Counterpropagating Pulsed Molecular-beam Scattering of NH_3-Ar . 2. State-resolved Differential Cross-sections. *J. Chem. Phys.* **1994,** *101*, 6697-6707.

(8) van der Sanden, G. C. M.; Wormer, P. E. S.; van der Avoird, A., Differential Cross Sections for Rotational Excitation of NH_3 by Collisions with Ar and He: Close Coupling Results and Comparison with Experiment. *J. Chem. Phys.* **1996,** *105*, 3079-3088.

(9) Schleipen, J.; ter Meulen, J. J.; van der Sanden, G. C. M.; Wormer, P. E. S.; van der Avoird, A., State-to-state Cross-sections for Rotational-excitation of Ortho-NH_3 and Para-NH_3 by Ar. *Chem. Phys.* **1992,** *163*, 161-172.

(10) Kay, J. J.; van de Meerakker, S. Y. T.; Wade, E. A.; Strecker, K. E.; Chandler, D. W., Differential Cross Sections for Rotational Excitation of ND_3 by Ne. *J. Phys. Chem. A* **2009,** *113*, 14800-14806.

(11) Yang, C. H.; Sarma, G.; ter Meulen, J. J.; Parker, D. H.; Buck, U.; Wiesenfeld, L., Imaging the Inelastic Scattering of Water with Helium. Comparison of Experiment and Theory. *J. Phys. Chem. A* **2010,** *114*, 9886-9892.

(12) Brudermann, J.; Steinbach, C.; Buck, U.; Patkowski, K.; Moszynski, R., Elastic and Rotationally Inelastic Differential Cross Sections for He+H_2O Collisions. *Journal of Chemical Physics* **2002,** *117*, 11166-11174.

(13) Yang, C. H.; Sarma, G.; Parker, D. H.; ter Meulen, J. J.; Wiesenfeld, L., State-to-state Differential and Relative Integral Cross Sections for Rotationally Inelastic Scattering of H_2O by Hydrogen. *J. Chem. Phys.* **2011,** *134*, 204308.

(14) Sarma, G.; Marinakis, S.; ter Meulen, J. J.; Parker, D. H.; McKendrick, K. G., Inelastic Scattering of Hydroxyl Radicals with Helium and Argon by Velocity-map Imaging. *Nature Chem.* **2012,** *4*, 985-989.

(15) Wade, E. A.; Lorenz, K. T.; Springfield, J. L.; Chandler, D. W., Collisions of HCl with Rare Gas and Molecular Colliders. *J. Phys. Chem. A* **2003,** *107*, 4976-4981.

(16) Elioff, M. S.; Chandler, D. W., State-to-state Differential Cross Sections for Spin-multiplet-changing Collisions of NO($X^2P_{1/2}$) with Argon. *J. Chem. Phys.* **2002,** *117*, 6455-6462.

(17) Eyles, C. J.; Brouard, M.; Chadwick, H.; Hornung, B.; Nichols, B.; Yang, C. H.; Kłos, J.; Aoiz, F. J.; Gijsbertsen, A.; Wiskerke, A. E.; *et al*., Fully Lambda-doublet Resolved State-to-state Differential Cross-sections for the Inelastic Scattering of NO(X) with Ar. *Phys. Chem. Chem. Phys.* **2012,** *14*, 5403-5419.

(18) Gijsbertsen, A.; Linnartz, H.; Rus, G.; Wiskerke, A. E.; Stolte, S.; Chandler, D. W.; Klos, J., Differential Cross Sections for Collisions of Hexapole State-selected NO with He. *J. Chem. Phys.* **2005,** *123*, 224305.

(19) Jons, S. D.; Shirley, J. E.; Vonk, M. T.; Giese, C. F.; Gentry, W. R., State-to-state Differential Cross-sections for Rotationally Inelastic Multiplet-conserving and Multiplet-changing Collisions of NO($^2P_{1/2}$, j=0.5) with Ar. *J. Chem. Phys.* **1992,** *97*, 7831-7834.

(20) Kohguchi, H.; Suzuki, T.; Alexander, M. H., Fully State-resolved Differential Cross Sections for the Inelastic Scattering of the Open-shell NO Molecule by Ar. *Science* **2001,** *294*, 832-834.

(21) Tkáč, O.; Sage , A. G.; Greaves, S. J.; Orr-Ewing, A. J.; Dagdigian, P. J.; Ma, Q.; Alexander, M. H., Rotationally Inelastic Scattering of CD_3 and CH_3 with He: Comparison of Velocity Map-Imaging Data with Quantum Scattering Calculations. *Chem. Sci.* **2013,** *4*, 4199 - 4211.

(22) Tkáč, O.; Ma, Q.; Rusher, C. A.; Greaves, S. J.; Orr-Ewing, A. J.; Dagdigian, P. J., Differential and Integral Cross Sections for the Rotationally Inelastic Scattering of Methyl Radicals with H_2 and D_2. *J. Chem. Phys.* **2014,** *140*, 204318.

(23) Tkáč, O.; Ma, Q.; Stei, M.; Orr-Ewing, A. J.; Dagdigian, P. J., Rotationally Inelastic Scattering of Methyl Radicals with Ar and N_2. *J. Chem. Phys.* in press **2015**.

(24) Tkáč, O.; Orr-Ewing, A. J.; Dagdigian, P. J.; Alexander, M. H.; Onvlee, J.; van der Avoird, A., Collision Dynamics of Symmetric Top Molecules: A Comparison of the Rotationally Inelastic Scattering of CD_3 and ND_3 with He. *J. Chem. Phys.* **2014,** *140*, 134308.

(25) von Zastrow, A.; Onvlee, J.; Vogels, S. N.; Groenenboom, G. C.; van der Avoird, A.; van de Meerakker, S. Y. T., State-resolved Diffraction Oscillations Imaged for Inelastic Collisions of NO Radicals with He, Ne and Ar. *Nat. Chem.* **2014,** *6*, 216-221.

(26) Gubbels, K. B.; van de Meerakker, S. Y. T.; Groenenboom, G. C.; Meijer, G.; van der Avoird, A., Scattering Resonances in Slow NH_3-He Collisions. *J. Chem. Phys.* **2012,** *136*, 074301.

(27) McBane, G. C., *Simulation of Crossed Beam Images (in Imaging in Chemical Dynamics)*. ACS Books: 2001.

(28) Eyles, C. J. An Experimental and Theoretical Study of the Dynamics of Atom-Molecule Scattering. D. Phil., University of Oxford, 2010.

(29) Loreau, J.; Liévin, J.; Scribano, Y.; van der Avoird, A., *J. Chem. Phys.* **2014**, *141*, 224303.
(30) Green, S., Rotational Excitation of Symmetric Top Molecules by Collisions with Atoms - Close Coupling, Coupled States, and Effective Potential Calculations for NH_3-He. *J. Phys. Chem.* **1976,** *64*, 3463-3473.
(31) Davis, S. L.; Boggs, J. E., Rate Constants for Rotational Excitation in NH_3-He Collisions. *J. Chem. Phys.* **1978,** *69*, 2355-2366.

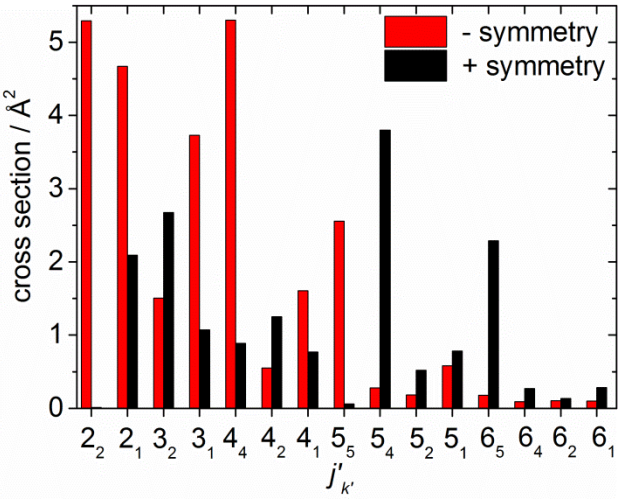

FIG. 1. Calculated integral cross sections for ND_3 collisions with Ar from $j_k^{\pm} = 1_1^-$ to various final rotational levels $j'_{k'}$ with – umbrella inversion symmetry (red) and + symmetry (black).

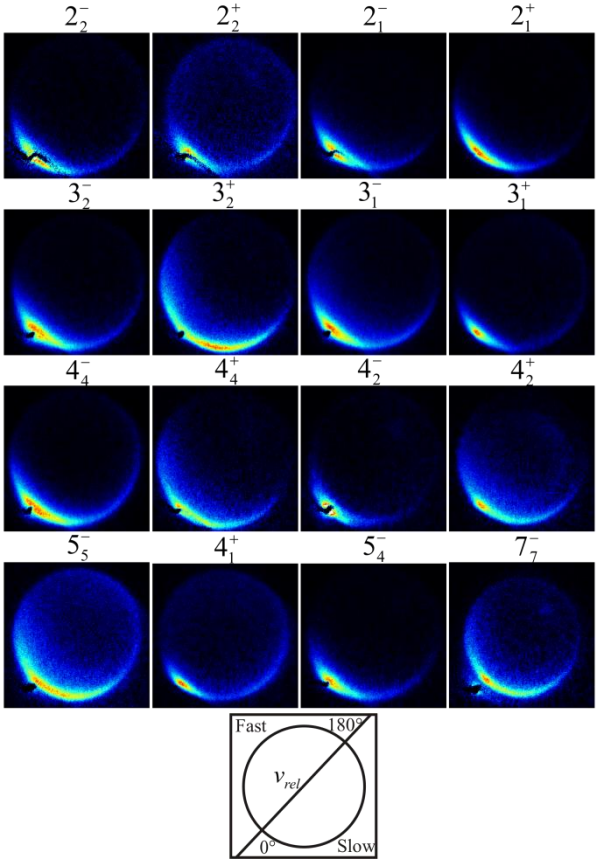

FIG. 2. Velocity map images for the inelastic scattering of ND_3 with Ar at a collision energy of 410 ± 40 cm^{-1}. The ND_3 was state-selected by a hexapole filter to be almost exclusively in the $j_k^{\pm} = 1_1^-$ state prior to collision.

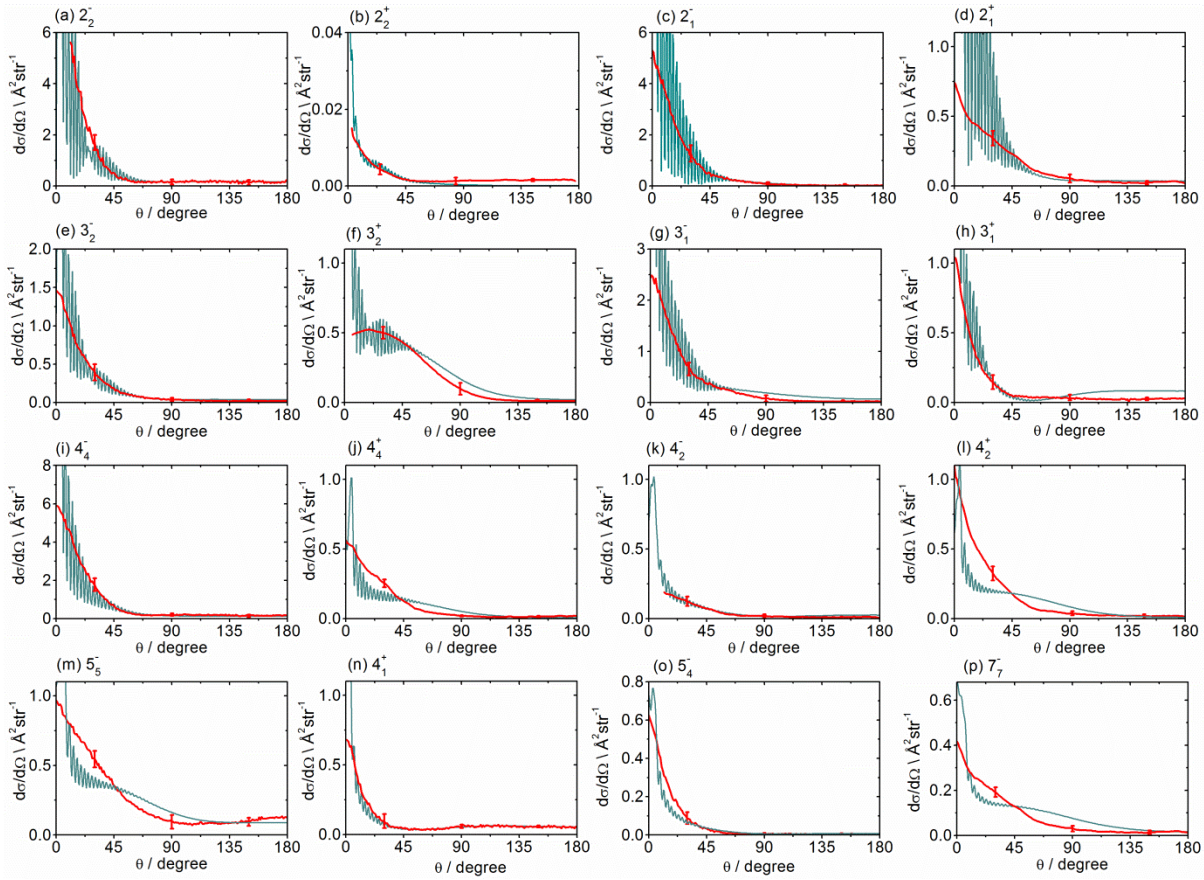

FIG. 3. Experimental (red) and theoretical (gray) DCSs for inelastic scattering of ND_3 $j_k^{\pm} = 1_1^-$ with Ar into various $j'^{\pm}_{k'}$ final levels. Experimental DCSs were derived from the raw images in Fig. 2 following density-to-flux transformation. The collision energy was 410 ± 40 cm^{-1}.

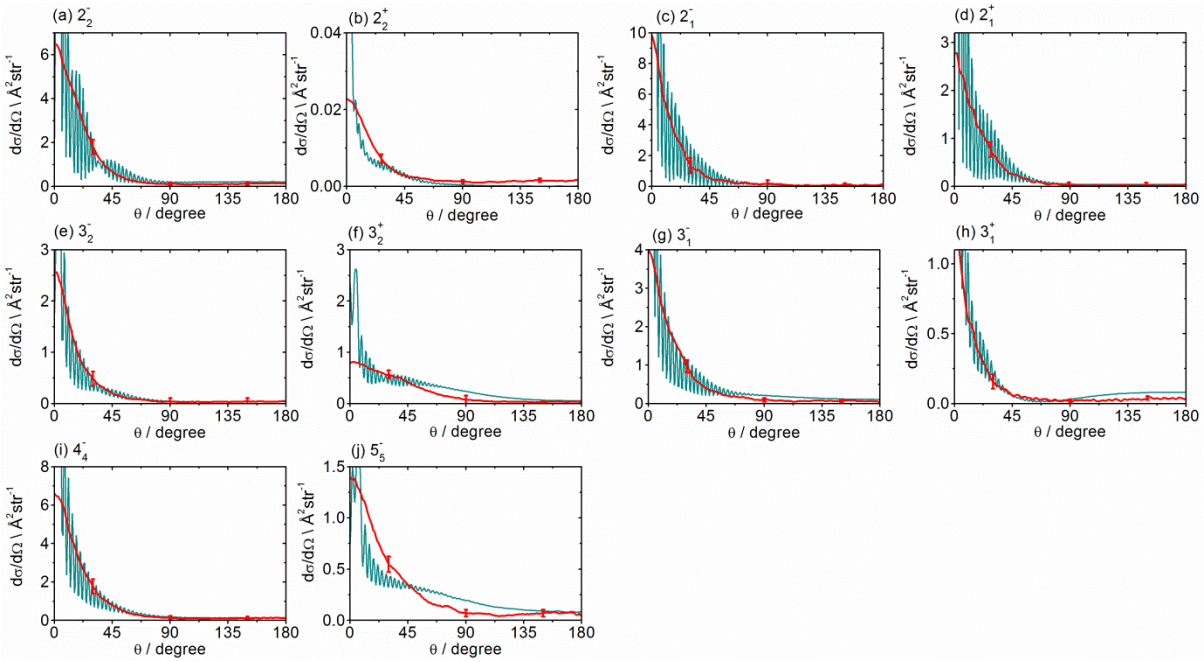

FIG. 4. Experimental (red) and theoretical (gray) DCSs for inelastic scattering of ND_3 $j_k^{\pm} = 1_1^-$ (seeded in Kr) with Ar into various $j'^{\pm}_{k'}$ final levels. Experimental DCSs were derived from the raw images in Fig. S3 following density-to-flux transformation. The collision energy was 310 ± 30 cm^{-1}.

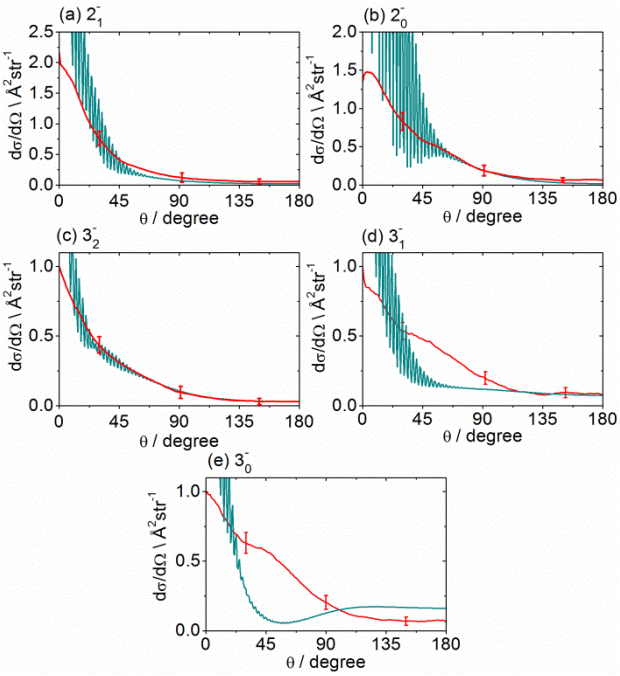

FIG. 5. Experimental (red) and theoretical (gray) DCSs for inelastic scattering of ND_3 (seeded in Ar) with Ar into various $j'^{-}_{k'}$ final levels. The hexapole state selection process was not used for this experiment. The final level 2_0^- corresponds to the A_2 modification and 3_0^- to the A_1 modification of ND_3. Experimental DCSs were derived from the raw images in Fig. S4 following density-to-flux transformation. The collision energy was 415 ± 40 cm^{-1}.

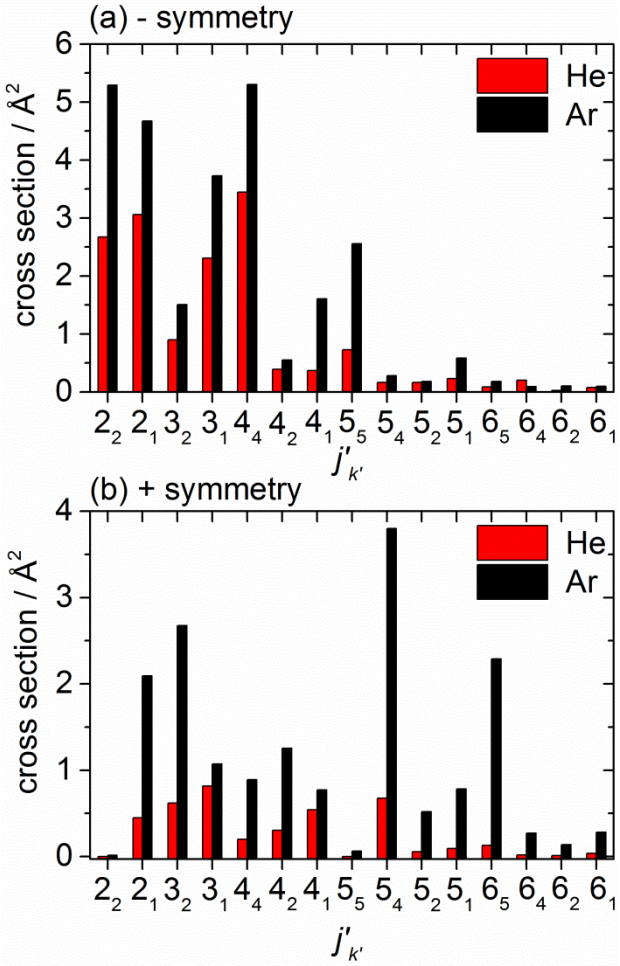

FIG. 6. Calculated integral cross sections for ND_3 collisions with Ar and He from $j_k^{\pm} = 1_1^-$ to various final rotational levels $j'_{k'}$ with (a) – umbrella inversion symmetry and (b) + symmetry. The collision energy for both systems was 410 cm^{-1}.

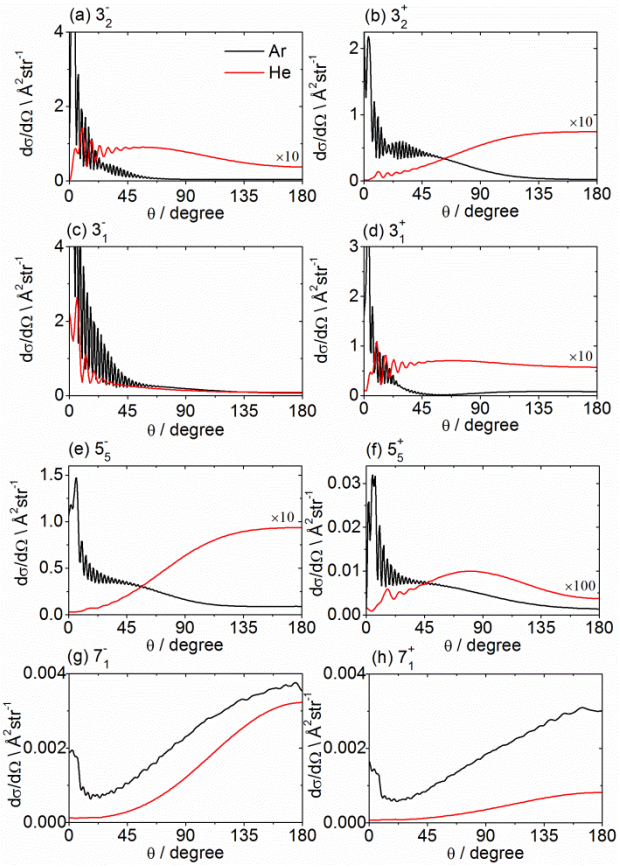

FIG. 7. Calculated DCSs for inelastic scattering of ND_3 $j_k^{\pm} = 1_1^-$ with Ar (black) and He (red) into selected $j'^{\pm}_{k'}$ final levels. The collision energy for both systems was 410 cm^{-1}.

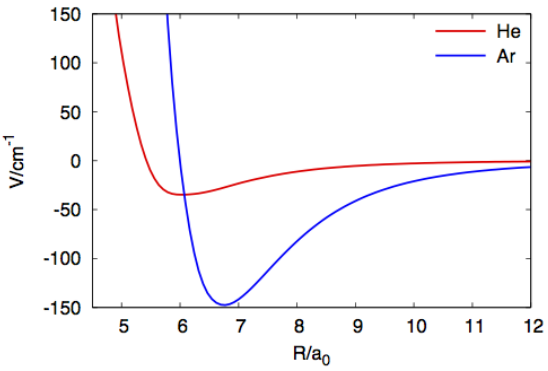

FIG. 8. Cuts through the minimum geometry for the ND_3 – Ar and ND_3 – He PESs.

Table of Contents Image